



Atmospheric propane (C_3H_8) column retrievals from ground-based FTIR observations at Xianghe, China

Minqiang Zhou¹, Pucai Wang¹, Bart Dils², Bavo Langerock², Geoff Toon³, Christian Hermans², Weidong Nan⁴, Qun Cheng⁴, and Martine De Mazière²

¹Institute of Atmospheric Physics, Chinese Academy of Sciences, Beijing, China

²Royal Belgian Institute for Space Aeronomy (BIRA-IASB), Brussels, Belgium

³Jet Propulsion Laboratory, California Institute of Technology, Pasadena, CA, USA

⁴Xianghe Observatory of Whole Atmosphere, Institute of Atmospheric Physics, Chinese Academy of Sciences, Xianghe, China

Correspondence: Minqiang Zhou (minqiang.zhou@mail.iap.ac.cn); Pucai Wang (pcwang@mail.iap.ac.cn)

Abstract. Propane (C_3H_8) is an important trace gas in the atmosphere, as it is a proxy for oil and gas production and has a significant impact on atmospheric chemical reactions related to the hydroxyl radical and tropospheric ozone formation. In this study, solar direct absorption spectra near 2967 cm^{-1} recorded by a ground-based Fourier Transform InfraRed spectrometer (FTIR) are applied to retrieve C_3H_8 total columns between June 2018 and July 2022 at Xianghe in North China. The systematic and random uncertainties of the C_3H_8 column retrieval are estimated to be 18.2% and 18.1%, respectively. The mean and standard deviation of the C_3H_8 columns derived from the FTIR spectra at Xianghe are $1.80 \pm 0.81(1\sigma) \times 10^{15}\text{ molecules/cm}^2$. Good correlations are found between C_3H_8 and other non-methane hydrocarbons, such as C_2H_6 ($R=0.84$) and C_2H_2 ($R=0.79$), as well as between C_3H_8 and CO ($R=0.72$). However, the correlation between C_3H_8 and CH_4 is relatively weak ($R=0.45$). The FTIR C_3H_8 measurements are also compared against two atmospheric chemical transport model simulations (the Whole Atmosphere Community Climate Model (WACCM) and the Copernicus Atmosphere Monitoring Service (CAM5)). We find that the C_3H_8 columns from both models have different seasonal variations as compared to the FTIR measurements. Moreover, the mean C_3H_8 columns derived from the WACCM and CAM5 models are about 68% larger than the FTIR retrievals. The new FTIR measurements at Xianghe provide us an insight into the C_3H_8 column variations and underlying processes in North China.

1 Introduction

Methane (CH_4) and non-methane hydrocarbons (NMHC), such as ethane (C_2H_6), acetylene (C_2H_2), propane (C_3H_8), propene (C_3H_6), and isoprene (C_5H_8), are important trace gases that play significant roles in atmospheric chemical reactions related to hydroxyl radical (OH) abundance and tropospheric ozone (O_3) formation (Sze, 1977; Donahue and Prinn, 1990; Tan et al., 2012; Lelieveld et al., 2015). Human activities contribute greatly to the emissions of CH_4 and NMHCs, especially in urban areas (Bourtsoukidis et al., 2019; Saunois et al., 2020). Atmospheric C_2H_6 and C_3H_8 emissions are dominated by oil and



gas sources, and they are co-emitted with CH₄. Therefore, numerous studies used the ratio of C₂H₆ and/or C₃H₈ to CH₄ to understand the CH₄ trend (Kort et al., 2016; Franco et al., 2016; Rigby et al., 2017).

The major sink of C₂H₆ and C₃H₈ is the reaction with OH, and the lifetime of C₃H₈ and C₂H₆ is about 2-4 weeks in summer and 2 months in winter (Jacob, 1999; Xiao et al., 2008). Compared to CH₄ with a lifetime of the order of 10 years (IPCC, 2013), the short-lived gases C₂H₆ and C₃H₈ are not well-mixed on the global scale, and are therefore more representative of regional pollution as is carbon monoxide (CO) (Toon et al., 2021).

Atmospheric C₃H₈ concentrations at the surface are observed by National Oceanic and Atmospheric Administration (NOAA) - Global Monitoring Laboratory (GML) flask sampling measurements at 12 sites (<https://gml.noaa.gov/hats/gases/C3H8.html>). In addition, the HIAPER Pole-to-Pole Observations (HIPPO), Atmospheric Tomography (ATom), and In-service Aircraft for a Global Observing System (IAGOS) aircraft campaigns provide in-situ gas analyzer measurements of C₃H₈ with a wide latitudinal coverage, particularly in the Pacific Ocean, Atlantic Ocean, Europe and North America (Wofsy, 2011; Thompson et al., 2022; Li et al., 2022). Toon et al. (2021) has demonstrated the use of C₃H₈ absorption lines in the mid-infrared region (Harrison et al., 2010), in solar absorption spectra from MkIV interferometers for retrieving the C₃H₈ total columns or vertical profiles at several locations in Sweden, the USA, and Antarctica. Solar absorption infrared spectra are also being collected by ground-based Fourier Transform Spectrometers (FTIR) within the Network for the Detection of Atmospheric Composition Change - InfraRed Working Group (NDACC-IRWG) (De Mazière et al., 2018). Currently, there are more than 20 NDACC-IRWG global sites, with a good global latitudinal coverage from 78°S to 80°N (<https://www2.acom.ucar.edu/irwg/sites>). However, to our knowledge, no site has reported C₃H₈ retrievals from spectra observed by a Bruker 125HR spectrometer within the NDACC-IRWG.

Xianghe (39.75 °N, 116.96 °E) is located in North China, about 50 km east of the mega-city Beijing (Yang et al., 2020). According to the Emissions Database for Global Atmospheric Research (EDGAR) v6.0 (Crippa et al., 2020) and the Multi-resolution Emission Inventory for China (MEIC) inventory (Wang et al., 2015; Li et al., 2017), there is a large CH₄ emission source in North China coming from fuel exploitation and oil refineries. Therefore, we expect that the C₂H₆ and C₃H₈ concentrations are relatively high in this region. In June 2018, a Bruker IFS 125HR spectrometer, compliant with the NDACC-IRWG protocol, started recording solar absorption spectra in the mid-infrared spectral range. The spectra have been used to retrieve several atmospheric components, e.g., O₃, CH₄, CO, C₂H₂, C₂H₆, HCN and H₂CO (Ji et al., 2020; Zhou et al., 2020, 2021, 2023; Vigouroux et al., 2020; Sha et al., 2021). In this study, we investigate the C₃H₈ retrieval from ground-based FTIR spectra at Xianghe, and discuss the C₃H₈ column variation in North China, based on these new FTIR measurements.

The remainder of this paper is organized as follows. Section 2 describes the Xianghe FTIR site and C₃H₈ retrieval method, Section 3 presents the C₃H₈ variations and correlations with other species. Moreover, the C₃H₈ measurements at Xianghe are compared to model simulations and ground-based MkIV measurements at other places. Finally, Section 4 draws a conclusion.



2 Method

2.1 Xianghe FTIR spectra measurement

The Xianghe FTIR measurement system started in June 2018, and has been well described in previous studies (Yang et al., 2020; Zhou et al., 2021, 2023). Briefly, the FTIR measurement system contains 3 parts: a solar tracker system, a weather station, and a Bruker IFS 125HR Fourier-transform infrared (FTIR) spectrometer. Short-Wave infrared (SWIR) and Near-infrared (NIR) spectra ($4000\text{--}11000\text{ cm}^{-1}$) with a spectral resolution of 0.02 cm^{-1} are recorded with an InGaAs detector, and these spectra are used to derive greenhouse gases total column abundances as a contribution to the Total Carbon Column Observing Network (TCCON). Mid-infrared (MIR) spectra ($1800\text{--}4500\text{ cm}^{-1}$), with a spectral resolution of $0.0035\text{--}0.0070\text{ cm}^{-1}$, are recorded with an InSb detector. To enhance the signal-to-noise ratio (SNR) of the spectra, we add specific optical filters into the light path when recording each MIR spectrum as recommended by NDACC-IRWG (Blumenstock et al., 2021; Zhou et al., 2023). A typical MIR spectrum used for C_3H_8 retrieval is shown in Figure 1. Note that, we only operate the FTIR measurement during the daytime and under clear-sky conditions, as the sun is the light source. In general, we carry out 4 to 10 MIR spectral measurements of this type per day for about 200 days per year. The spectra taken between June 2018 and July 2022 (about 4 years) are used in this study.

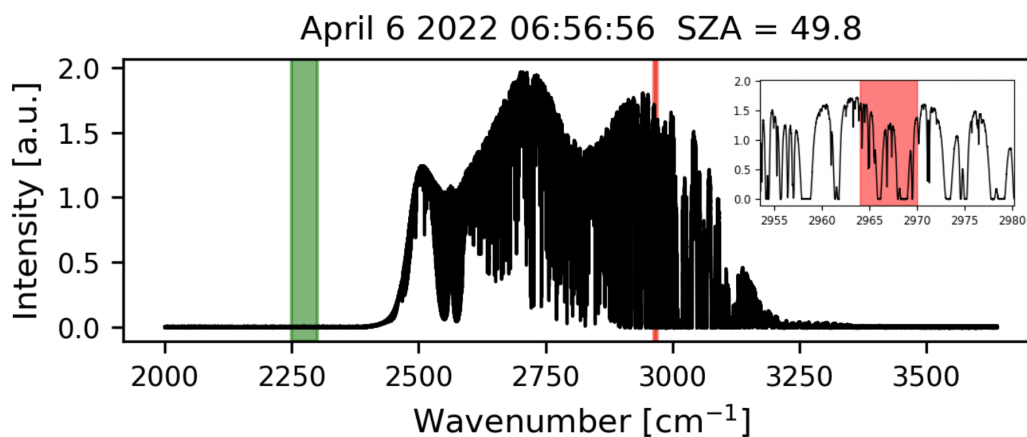


Figure 1. A typical MIR spectrum observed at Xianghe on 6 April 2022 with a solar zenith angle of 49.8° . The red and green windows indicate the micro-windows windows used for the C_3H_8 retrieval and for calculating the noise (Eq. 5), respectively. The insert in the right-hand corner shows a zoom on the retrieval micro-window.

2.2 Retrieval method

To derive C_3H_8 mole fractions from the observed spectra, we follow the optimal estimation methodology (Rodgers, 2000). The forward model (**F**) simulates the absorption spectra (**y**) observed by the FTIR system. It includes modelling of the solar spectra at the top of the atmosphere (TOA), the physics of the radiative transfer from the TOA to the ground-based FTIR, and



the FTIR spectrometer line shape function (ILS). Then, the observed spectra (\mathbf{y}) can be written as

$$\mathbf{y} = \mathbf{F}(\mathbf{x}, \mathbf{b}) + \boldsymbol{\epsilon}, \quad (1)$$

where \mathbf{x} is the state vector (retrieved parameters), \mathbf{b} is the forward model parameters (not retrieved), and $\boldsymbol{\epsilon}$ is the error, including the measurement noise and forward model errors. We wish to find the optimal state (\mathbf{x}) that minimize the cost function ($\mathbf{J}(\mathbf{x})$),

5 given by

$$\mathbf{J}(\mathbf{x}) = [\mathbf{y} - \mathbf{F}(\mathbf{x})]^T \mathbf{S}_\epsilon^{-1} [\mathbf{y} - \mathbf{F}(\mathbf{x})] + [\mathbf{x} - \mathbf{x}_a]^T \mathbf{S}_R [\mathbf{x} - \mathbf{x}_a], \quad (2)$$

where \mathbf{S}_ϵ is the measurement error covariance matrix; \mathbf{S}_R is the regularization matrix; \mathbf{x}_a is the *a priori* state vector. The Levenberg-Marquardt (LM) method is used to iteratively solve the above equation:

$$\mathbf{x}_{i+1} = \mathbf{x}_i + [(1 + \gamma)\mathbf{S}_R + \mathbf{K}_i^T \mathbf{S}_\epsilon^{-1} \mathbf{K}_i]^{-1} \{ \mathbf{K}_i^T \mathbf{S}_\epsilon^{-1} [\mathbf{y} - \mathbf{F}(\mathbf{x}_i)] - \mathbf{S}_R [\mathbf{x}_i - \mathbf{x}_a] \}, \quad (3)$$

10 where \mathbf{K} is the Jacobian matrix, γ is a parameter to adjust the regularization of a priori information in each iteration step (Rodgers, 2000). Upon convergence, the final state is called \mathbf{x}_r , which can be related to the true state (\mathbf{x}_t):

$$\mathbf{x}_r = \mathbf{x}_a + \mathbf{A}(\mathbf{x}_t - \mathbf{x}_a) + \boldsymbol{\varepsilon}, \quad (4)$$

where \mathbf{A} is the averaging kernel matrix, representing the sensitivity of the retrieved parameters to the true parameter, and $\boldsymbol{\varepsilon}$ is the retrieval uncertainty propagated from Eq.1.

15 2.3 Retrieval strategy

In this study, we use the SFIT4 v1.0 retrieval algorithm (Pougatchev et al., 1995; Hase et al., 2004) to perform the forward model simulation as well as the LM inversion. The well-established SFIT4 code has been used extensively to retrieve total/partial column of atmospheric species in the NDACC-IRWG community (Zhou et al., 2016; De Mazière et al., 2018; Ortega et al., 2019).

20 The key C_3H_8 retrieval parameters used in this study are listed in Table 1. The retrieval window is set to 2964.5-2970.0 cm^{-1} , where we have the strongest C_3H_8 absorption line (Harrison et al., 2010). Apart from C_3H_8 , several interfering gases (H_2O , CH_4 , O_3 , and HDO) also have absorption lines in this window as shown in Figure 2. To reduce the impact of uncertainties about the abundances of these species, these column abundances are retrieved along with the target gas mole fractions; only for H_2O we perform a profile retrieval, because of its large variability.

25 The chosen spectroscopic parameters are crucial in the remote sensing technique. In this study, we have tested several line lists, particularly for H_2O (HDO) and CH_4 (see Table 2), including DLR2016 (Loos et al., 2017), HITRAN2020 (Gordon et al., 2022) and ATM2020 (<https://mark4sun.jpl.nasa.gov/pseudo.html>). The ATM2020 line list is created by Geoff Toon (NASA, JPL) based on HITRAN2020 together with some additional atmospheric and laboratory measurements. It includes pseudo linelists (PLL) for certain species as the ones we use for C_3H_8 , based on laboratory cross section measurements by Harrison et al. (2010). For C_2H_6 , we use HITRAN2020. We tested more than 1000 spectra recorded in 2019 at Xianghe, and we observed

30



that the lowest root-mean-square error (RMSE) of the fitting residual is obtained when the ATM2020 spectral database is used for CH₄ and H₂O. Table 1 lists the spectral datasets finally used for each species in the C₃H₈ retrieval strategy.

Table 1. The retrieval window, interfering specie, spectroscopy, fitting parameters for C₃H₈ at Xianghe.

Parameters	settings
Retrieval window (cm ⁻¹)	2964.5-2970.0
Profile retrieval species	C ₃ H ₈ , H ₂ O
Column retrieval species	C ₂ H ₆ , CH ₄ , HDO
Retrieved parameters	slope, phase, instrument line shape, wavenumber shift solar intensity, solar wavenumber shift
A priori profile	NCEP for H ₂ O, HDO; WACCM for C ₂ H ₆ , C ₃ H ₈ , CH ₄
Spectroscopy	PLL for C ₃ H ₈ ; ATM20 for H ₂ O, HDO, CH ₄ ; HITRAN2020 for C ₂ H ₆
Regularization	Tikhonov L ₁ method
DOFS	1.1

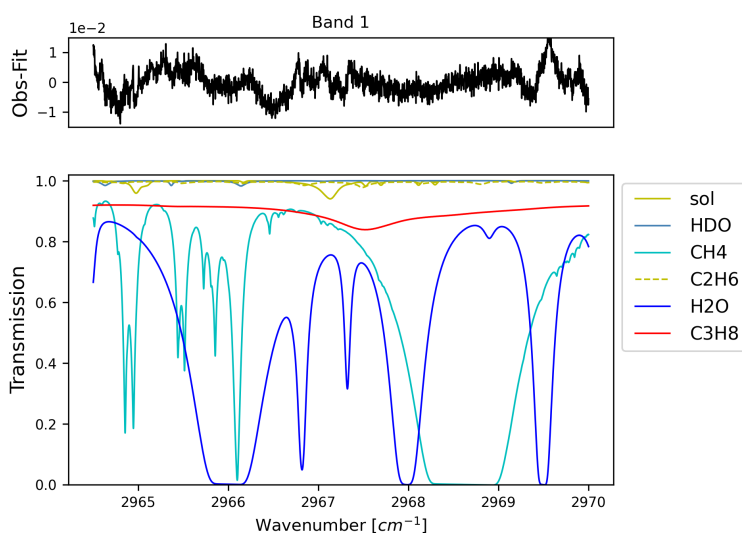


Figure 2. The transmittances of main species and solar lines (bottom), as well as the fitting residual (top) using the typical spectrum shown in Figure 1 in this retrieval window.

The *a priori* profiles for C₃H₈, C₂H₆, and CH₄ are derived from the Whole Atmosphere Community Climate Model (WACCM) version 6. We use the averages of the monthly means between 1980 and 2040 (61 years) as the *a priori* profiles. Since the variations of temperature and humidity are quite large in the atmosphere, using fixed *a priori* profiles often



Table 2. The fitting RMSE of the retrieval window for all spectra in 2019 from several different line lists.

H ₂ O (HDO)	CH ₄	RMSE (mean±1σ)
ATM2020	ATM2020	0.925±0.241
HITRAN2020	ATM2020	0.967±0.267
DLR	ATM2020	0.968±0.267
ATM2020	HITRAN2020	1.233±0.281
HITRAN2020	HITRAN2020	1.314±0.289

results in a bad fitting, especially for the first iteration. To provide a better estimation of temperature and humidity profiles, for each measurement, the H₂O (HDO) and temperature vertical profiles are derived from the closest 6-hourly NCEP reanalysis data (Saha et al., 2014), and linearly interpolated to the measurement time.

According to Eq.2, the cost function $J(x)$ is composed of the measurement and *a priori* information, each contracted with a weight matrix S_ϵ and S_R , respectively. In this study, the diagonal of the S_ϵ is calculated as $1/\text{SNR}^2$, and the non-diagonal values are set to 0. The SNR is calculated as

$$\text{SNR} = \frac{\overline{I_r}}{\sigma_{I_n}}, \quad (5)$$

where $\overline{I_r}$ is the max radiation intensity in the C₃H₈ retrieval window (2964.5-2970.0 cm⁻¹; red window in Figure 1) and σ_{I_n} is the standard deviation (std) of the intensity in the noise window (2250.0-2300.0 cm⁻¹; green window in Figure 1). The

Tikhonov L_1 regularization method (Tikhonov, 1963) is applied to generate the S_R , with

$$S_R = \alpha L_1^T L_1, \quad (6)$$

$$L_1 = \begin{bmatrix} -1 & 1 & 0 & \dots & 0 & 0 \\ 0 & -1 & 1 & \dots & 0 & 0 \\ \vdots & \vdots & \vdots & \ddots & \vdots & \vdots \\ 0 & 0 & 0 & \dots & -1 & 1 \end{bmatrix}. \quad (7)$$

To determine the α value in Eq. 6, we apply the degree of freedom for signal (DOF) method proposed by Steck (2002). The trace of the averaging kernel matrix (\mathbf{A}) is the DOF, indicating the pieces of independent information of the retrieval (Rodgers, 2000). First, we use the optimal estimation method (OEM) to get an estimated DOF. S_R using the OEM is derived from a covariance matrix on the WACCM monthly means between 1980 and 2040 ($S_{R_{i,i}} = S_{i,i}^{-1} = \sigma_i^{-2}$; diagonal values), and the non-diagonal values are set as

$$S_{R_{i,j}}^{-1} = S_{i,j} = e^{(d_{i,j}/4)} / (\sigma_i \sigma_j), \quad (8)$$

where $d_{i,j}$ is the vertical distance between layer i and layer j , in km. The DOF derived from the OEM is about 1.1, indicating that there is only column information for the C₃H₈ retrieval. Knowing that, we tune the α value in Eq.6 to make the DOF derived from the Tikhonov method close to the DOF that is derived from the OEM; this approach results in setting α to 1000.



2.4 Retrieval uncertainty

The retrieval error (ϵ) of the FTIR C_3H_8 column contains three parts as

$$(\mathbf{A} - \mathbf{I})(\mathbf{x}_t - \mathbf{x}_a) \quad \dots \quad \text{smoothing error} \quad (9)$$

$$\mathbf{G}_y \mathbf{K}_b (\mathbf{b}_t - \mathbf{b}_a) \quad \dots \quad \text{model parameter error} \quad (10)$$

$$5 \quad \mathbf{G}_y \epsilon \quad \dots \quad \text{measurement error} \quad (11)$$

where \mathbf{G}_y is the contribution function; \mathbf{b}_t and \mathbf{b} are the true and used model inputs, respectively. Table 3 lists the systematic and random uncertainty of each component. For the smoothing error, we separate the contributions into target species (C_3H_8), interfering species (H_2O , HDO , CH_4 , C_2H_6), and retrieved parameters (slope, phase, wavenumber shift, instrument line shape, solar intensity and shift). For the model parameter contributions, we calculate the C_3H_8 uncertainty contribution coming from spectroscopy, solar zenith angle (SZA), temperature profile, curvature parameter, and zero level shift (zshift). The systematic and random uncertainties of each parameter are also listed in Table 3. The vertical distributions of the systematic and random uncertainties are shown in Figure 3. Note that the spectroscopy uncertainty in Table 3 is the sum of the uncertainties from the line intensity, pressure-dependent parameter (linePAir) and temperature-dependent parameter (lineTAir). Based on our uncertainty estimation, the total systematic and random uncertainty of the C_3H_8 column are both about 18%, and the dominating contribution is the uncertainty on the background curvature parameter in the forward model. To represent the variability of the C_3H_8 , we select all days with at least 3 individual measurements on each day, and calculate the daily std. The average of all the daily stds is about 15.3%, and it is close to our estimated random uncertainty.

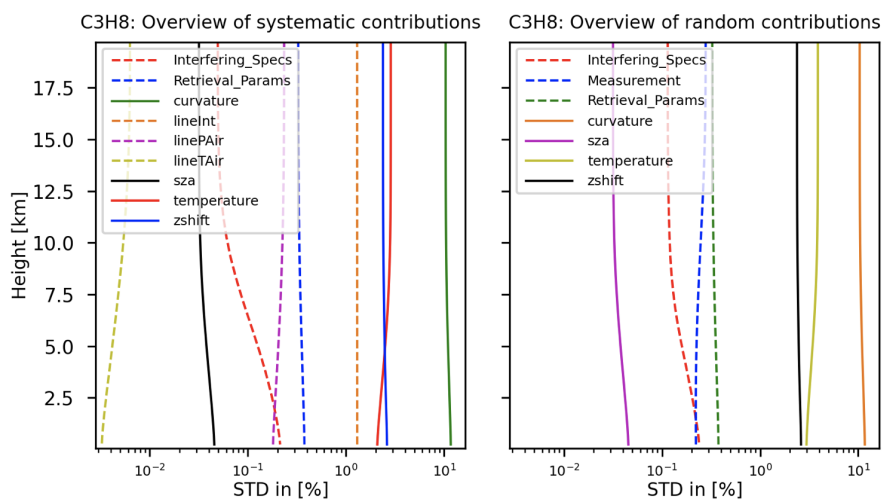


Figure 3. The vertical profiles of the systematic (left) and random error (right) of the FTIR C_3H_8 retrieval from each component.



Table 3. The systematic and random (sys/ran) retrieval uncertainties for the total columns of C_3H_8 . The ‘-’ means that the uncertainty is less than 0.1%. 1σ of the target or interfering species is the std derived from the WACCM model monthly means between 1980 and 2040. The relative std in the bottom row is the average of daily std of C_3H_8 columns on all days with at least 3 measurements, which is to represent the variability of the retrieval.

Error source	Parameter	Parameter uncertainty (sys/ran)	C_3H_8 column uncertainty [%]
Smoothing error	Target species	10/1 σ %	0.2/0.5
	Interfering species	10/1 σ %	0.7/0.6
	Retrieved parameters		0.6/0.6
Model parameter error	Spectroscopy	4.0/- %	4.1/-
	SZA	0.03/0.03°	0.1/0.1
	Curvature	0.1/0.1 %	17.2/17.2
	Temperature	1.5/2.0 K	2.7/3.9
	Zshift	0.15/0.15 %	2.9/2.9
Measurement error		$-\frac{1}{SNR}$	-/1.0
Total			18.2/18.1
Std			-/15.3

3 Results and discussions

3.1 FTIR C_3H_8 retrievals at Xianghe

Figure 4 shows the *a priori* profile and retrieved profiles of C_3H_8 . The vertical profile of C_3H_8 from the WACCM model shows that the C_3H_8 mole fraction is high near the surface and decreases with increasing altitude. Such a vertical shape is expected as the C_3H_8 emissions are at the surface, and its atmospheric lifetime is too short to achieve a well-mixed troposphere. Although we perform a profile retrieval on C_3H_8 , we only have about 1 DOF. In addition, the Tikhonov regularization matrix constrains the vertical shape when the DOF is typically close to 1.0. As a result, the retrieved C_3H_8 profiles have a very similar vertical shape as the *a priori* profile. However, the FTIR measurements show that the *a priori* column overestimates the C_3H_8 column concentration by about 100%. The column averaging kernel indicates the sensitivity of the retrieved C_3H_8 column to the C_3H_8 partial column in each height. Figure 4 shows that the retrieved C_3H_8 column has good sensitivity to all the layers, and slightly varies with SZA.

The time series and seasonal variation of FTIR C_3H_8 column measurements are presented in Figure 5. To better visualize the seasonal variation, the column measurements are fitted by a periodic function $y(t) = A_0 + \sum_{k=1}^3 (A_{2k-1} \cos(2k\pi t) + A_{2k} \sin(2k\pi t))$, where A_0 is the offset, and A_1 to A_6 are the periodic amplitudes, representing the seasonal variation. The obtained mean and std of C_3H_8 columns at Xianghe are $1.80 \pm 0.81 \times 10^{15} \text{ molec./cm}^2$. The C_3H_8 columns show a high

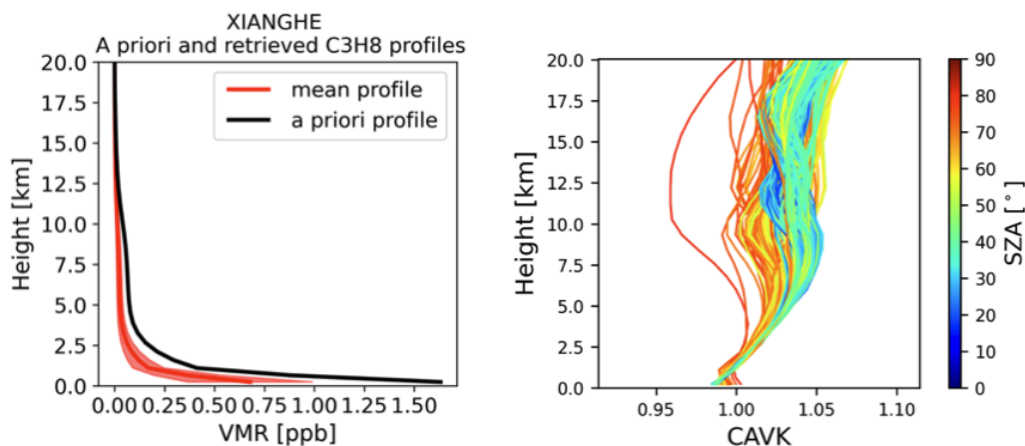


Figure 4. The *a priori* and retrieved C_3H_8 profiles (left), and the column averaging kernel (CAVK) varying with SZA (right).

mean value in July and a low value in October. The difference between the median values in July (maximum) and October (minimum) is $1.2 \times 10^{15} \text{ molec./cm}^2$. Although the median values of C_3H_8 columns in June–August are larger than those in October–March, we notice that extremely high C_3H_8 columns often occur in the latter period.

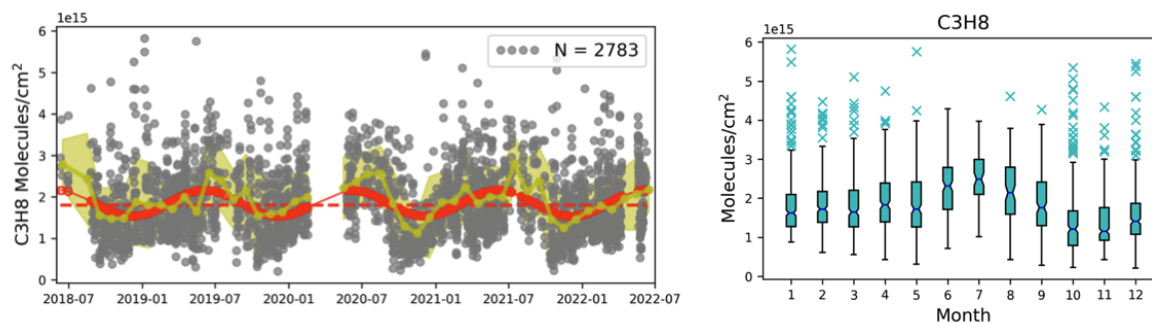


Figure 5. Left panel shows the time series of FTIR individual C_3H_8 column measurements (grey dots), monthly means (yellow line), monthly stds (yellow shade), periodic function fitting (red solid line) and the fitted offset (red dashed line). Right panel: the monthly box plot of the C_3H_8 columns. The bottom and top bars represent the 10% and 90% percentiles of the datasets and the blue crosses are the extremely high values above 90%.

3.2 FTIR C_3H_8 measurements against model simulations

- In this section, we compare the FTIR C_3H_8 measurements at Xianghe with two well-known global atmospheric chemistry transport models: WACCM and Copernicus Atmosphere Monitoring Service (CAMS). The WACCM model has been widely used to generate *a priori* profiles in the NDACC-IRWG community, spanning an altitude range from the Earth’s surface to the



thermosphere (Marsh et al., 2013; Gettelman et al., 2019). The horizontal resolution of the WACCM is $0.95^\circ \times 1.25^\circ$, with 70 vertical levels from the surface to 120 km. More information about the WACCM v6 model can be found in <https://www2.acom.ucar.edu/gcm/waccm>. The CAMS model (EAC4) is the fourth generation ECMWF global reanalysis of atmospheric composition, which combines model data with observations across the world. The horizontal resolution of the CAMS is $0.75^\circ \times 0.75^\circ$, with 60 model levels from the surface to ~ 0.1 hPa. For more information about the CAMS model, we refer to Inness et al. (2019).

Figure 6 shows the monthly C_3H_8 column distributions derived from FTIR measurements, the WACCM model, and the CAMS model at Xianghe between June 2018 and December 2022. The mean and std of C_3H_8 column derived from CAMS and WACCM are $3.07 \pm 1.37 \times 10^{15} \text{ molec./cm}^2$, and $3.00 \pm 1.08 \times 10^{15} \text{ molec./cm}^2$, respectively. The mean C_3H_8 columns from CAMS and WACCM models are similar, but both models are about 68% larger than the FTIR measurement. The mean difference between the model and FTIR C_3H_8 column is larger than the systematic uncertainty of the FTIR retrieval ($\sim 18\%$). Moreover, the seasonal variations of C_3H_8 columns derived from the CAMS and WACCM models are different from the one derived from the FTIR measurements. CAMS and WACCM both show a low C_3H_8 column in summer, when the FTIR measurements present the maximum median C_3H_8 column. The seasonal variation of C_3H_8 at JPL ($34^\circ N$) derived from the ground-based MKIV spectrometer also observes a high value in summer (Toon et al., 2021), which is similar to the C_3H_8 seasonal variation derived from the FTIR measurements at Xianghe ($39^\circ N$). Such a difference in seasonal variation between the FTIR measurements and model simulations might due to the uncertainty of emissions, transports, chemical reactions, and sinks.

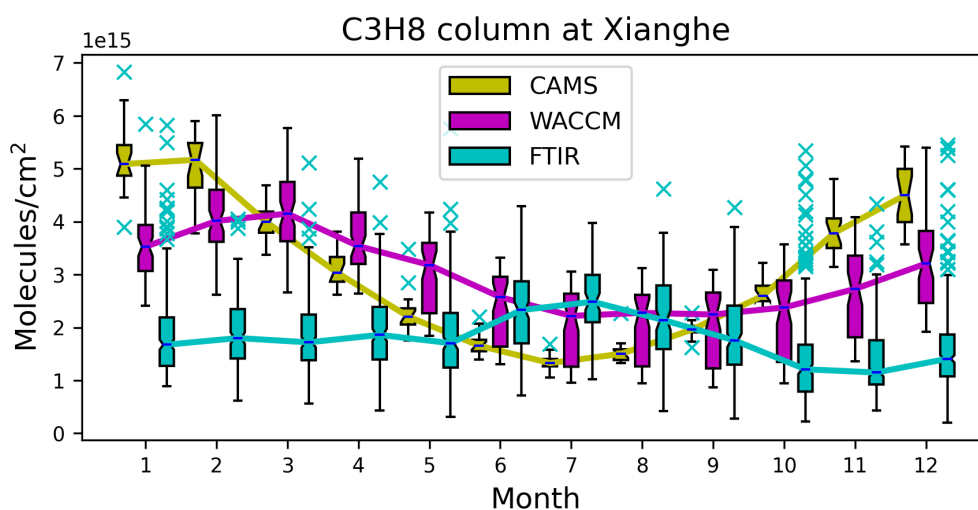


Figure 6. The monthly box plot of the C_3H_8 columns derived from the CAMS model, the WACCM model, and the FTIR measurements at Xianghe between June 2018 and December 2021.



3.3 Correlations with CO, CH₄, C₂H₂ and C₂H₆ at Xianghe

As mentioned above, the infrared spectra observed by the Xianghe FTIR system have been also used to retrieve CO, CH₄, C₂H₂ and C₂H₆ columns using NDACC-IRWG recommended retrieval recipes (Ji et al., 2020; Zhou et al., 2023), which allows us to investigate the correlation between C₃H₈ and these species. We are particularly interested in the correlation on a regional
5 scale. Therefore, to reduce the impact from the background, we calculate the Δ_{gas} ($\Delta_{\text{gas}} = \text{gas} - \text{monthly median}$) for all these species. Figure 7 shows the correlation scatter plots between $\Delta_{\text{C}_3\text{H}_8}$ and Δ_{CH_4} , Δ_{CO} , $\Delta_{\text{C}_2\text{H}_2}$, and $\Delta_{\text{C}_2\text{H}_6}$. High correlation coefficients (R) are found between $\Delta_{\text{C}_3\text{H}_8}$ and $\Delta_{\text{C}_2\text{H}_6}$ (R=0.84), and between $\Delta_{\text{C}_3\text{H}_8}$ and $\Delta_{\text{C}_2\text{H}_2}$ (R=0.79). It indicates that the C₂H₂, C₂H₆ and C₃H₈ (NMHCs) are co-emitted in this region. The slope of $\Delta_{\text{C}_2\text{H}_6}$ and $\Delta_{\text{C}_3\text{H}_8}$ is 6.03 ± 0.03 , which suggests a corresponding mixing ratio of C₂H₆ and C₃H₈ mole fractions during the production in North China. CO, as a
10 pollutant tracer, also has a good correlation with C₃H₈ (R=0.72). According to the MEIC inventory, both CO and NMHC are emitted from the energy production, industry, residential and transport sectors.

The FTIR measurements show that the correlation between $\Delta_{\text{C}_3\text{H}_8}$ and Δ_{CH_4} is relatively weak (R=0.45). Note that the variation of the CH₄ column is also affected by the stratospheric partial column (Sepúlveda et al., 2014). The DOF of the FTIR CH₄ retrieval is about 2.5 allowing us to derive the tropospheric and stratospheric CH₄ partial columns separately (Zhou
15 et al., 2018). However, even after eliminating the interference from the stratosphere, the tropospheric CH₄ partial column still have a weak correlation with C₃H₈ (R=0.43). It is probably due to that the CH₄ major emissions in North China are from rice cultivation, waste, and animals instead of the oil and gas production (Ji et al., 2020), and the CH₄ measurements include the emissions from much farther away as compared to the C₃H₈ measurements because of its long lifetime (Callewaert et al., 2023).

To further investigate the ratio of $\Delta_{\text{C}_2\text{H}_6}$ to $\Delta_{\text{C}_3\text{H}_8}$, the time series of their ratios, together with the monthly correlation coefficients between both time series between June 2018 and June 2022 are illustrated in Figure 8. The ratio of each month is derived from the linear fitting using all co-located $\Delta_{\text{C}_2\text{H}_6}$ and $\Delta_{\text{C}_3\text{H}_8}$ hourly measurements in that month. A relatively low correlation between these two species is found in summer as compared to other three seasons. The mean and std of the ratios are 5.4 ± 2.1 for the whole period. The ratio is lowest in summer and highest in winter, with seasonal means of 6.6, 3.8, 5.4,
20 and 8.3 in spring, summer, autumn, and winter, respectively.

3.4 FTIR measurements at Xianghe against MkIV measurements

Here, the C₃H₈ and C₂H₆ columns derived from the FTIR measurements at Xianghe are compared to the ground-based MkIV C₃H₈ retrievals at 6 sites in Sweden and the USA (Figure 9). Note that the C₃H₈ and C₂H₆ retrievals from the MkIV spectrometers at 12 sites have been discussed in Toon et al. (2021), we only select 6 sites as the measurements are very limited at
30 other 6 sites. The locations and measurement time coverages of sites used in this study are listed in Table 4.

Figure 9 shows that the C₂H₆ column is the largest at Xianghe, apart from several extremely high values at JPL-B and FTS. The seasonal variations of C₂H₆ columns are similar at these sites, especially for JPL-B, MTB and Xianghe, with a high value in northern spring and a low value in northern autumn. Note that, it is hard to derive the seasonal variation of C₂H₆ columns

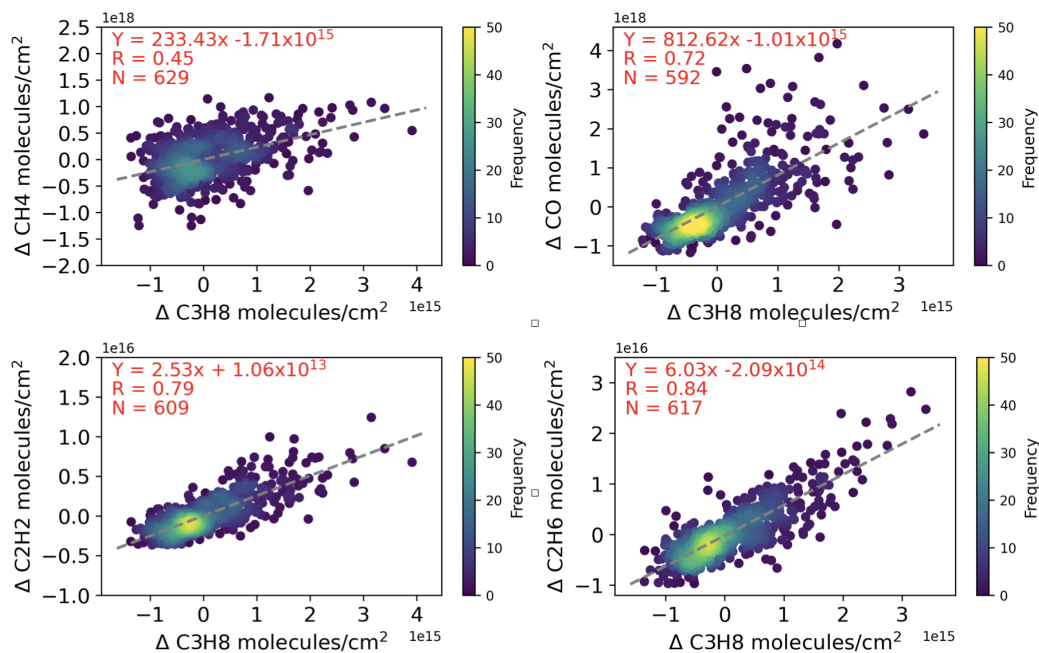


Figure 7. The correlation plots between co-located ΔC_3H_8 and ΔCH_4 , ΔCO , ΔC_2H_2 and ΔC_2H_6 hourly means at Xianghe between June 2018 and July 2022. The grey dashed line is the linear fit, N is the number of the FTIR measurements, R is the Pearson correlation coefficient.

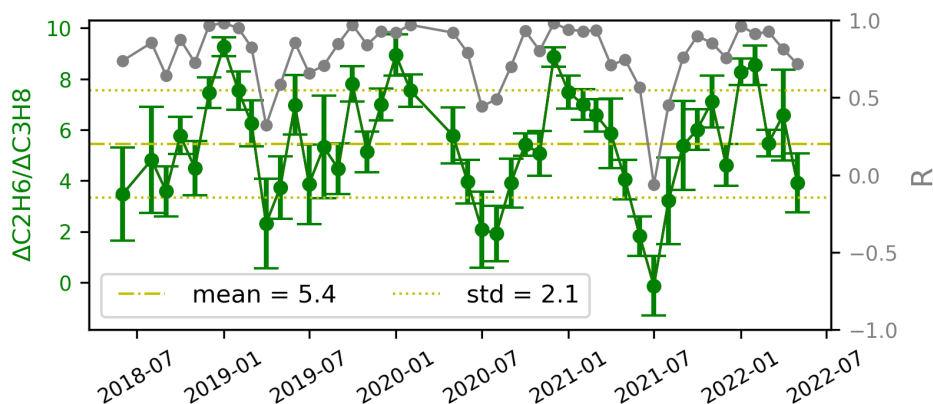


Figure 8. The time series of the ratio of ΔC_2H_6 to ΔC_3H_8 monthly means and stds (green, on the left-hand vertical axis scale), together with their monthly correlation coefficients (grey, on the right-hand vertical axis scale) between June 2018 and June 2022.

at ESN, FAI, TMF and FTS, because measurements were carried out in several months. The mean and std of C₂H₆ columns at JPL-B are $1.96 \pm 0.52 \times 10^{16} \text{ molec./cm}^2$, which is about 25% less than that at Xianghe ($(\text{Xianghe-JPL})/\text{Xianghe} \times 100\%$). Keep in mind that the C₃H₈ columns at MTB and Xianghe have been multiplied by 10 in Figure 9. The C₃H₈ column at



Xianghe is quite low as compared to other sites, which is only larger than that at MTB (mountain site), but much less than those at the mid-latitude sites. The mean and std of C_3H_8 columns at JPL-B are $2.14 \pm 1.33 \times 10^{16} \text{ molec./cm}^2$, which is about 12 times larger than that at Xianghe. The seasonal variations of C_3H_8 columns are similar at JPL-B and Xianghe too, with a high value in northern summer and a low value in northern winter. The good correlations ($R > 0.6$) between C_3H_8 and C_2H_6 columns at JPL-B and FTS have been demonstrated in Toon et al. (2021), which is similar to what we observe at Xianghe. However, the ratio of ΔC_2H_6 to ΔC_3H_8 at JPL-B and FTS are 0.16 ± 0.10 and 0.78 ± 0.10 , respectively, which are much less than the ratio observed at Xianghe of 6.03 ± 0.03 . It indicates that the emission of C_3H_8 is much larger in the Los Angeles basin, California than that in North China.

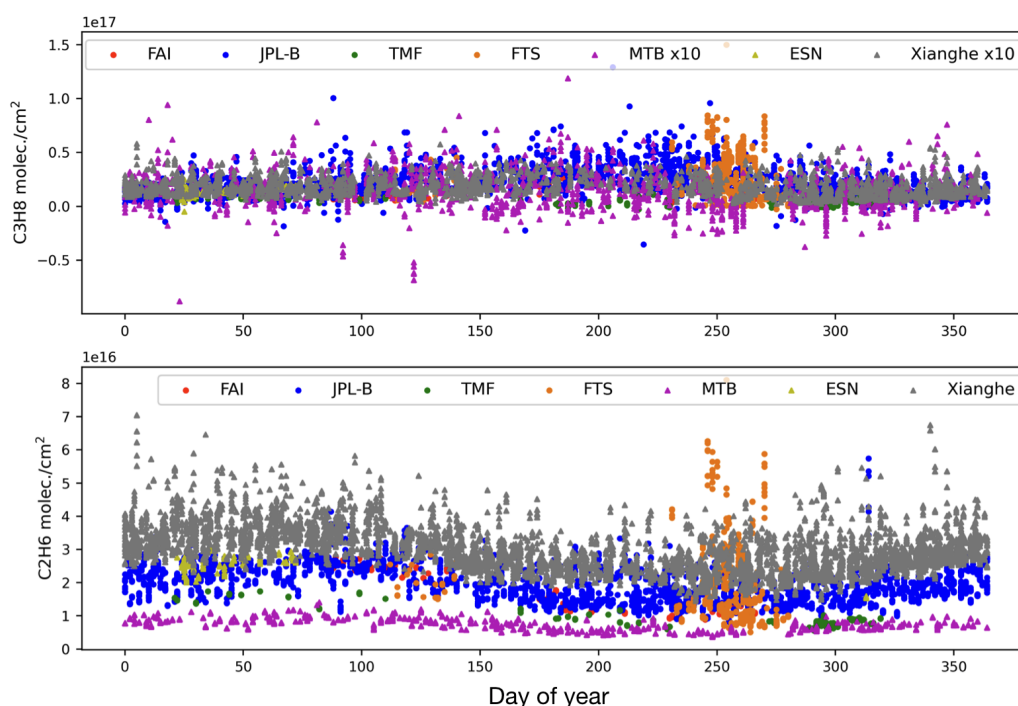


Figure 9. The C_3H_8 (upper panel) and C_2H_6 (lower panel) columns observed by ground-based Bruker IFS 125HR at Xianghe and MkIV spectrometer at 6 sites. Note that the C_3H_8 columns observed at MTB and Xianghe are multiplied by 10 to have a better view.

4 Conclusions

10 The Xianghe FTIR 125HR system measures the solar absorption spectra following the NDACC-IRWG guidance. For the first time, the FTIR MIR spectra at Xianghe are used for the C_3H_8 column retrieval, using the well-established SFIT4 code, between June 2018 and July 2022. In this study, the retrieval strategy, retrieval uncertainty, and retrieval information are presented and discussed. Due to the wide and weak absorption of C_3H_8 , we only derive the C_3H_8 column instead of its vertical profile. The



Table 4. The locations, and data time coverages of the MkIV measurements at 6 sites, together with their mean C_3H_8 and C_2H_6 columns. The bottom row is the Xianghe FTIR measurements in this study.

Site	Country	Latitude	Longitude	Altitude (km)	Time coverage	C_3H_8 (molec./cm ²)	C_2H_6 (molec./cm ²)
Esrang(ESN)	Sweden	67.89°N	21.08°E	0.271	Nov 1999 - Mar 2020	1.4×10^{16}	2.6×10^{16}
Fairbanks(FAI)	USA	64.83°N	147.61°W	0.182	Mar-Sep 1997	1.4×10^{16}	1.8×10^{16}
Mt. Barcroft(MTB)	USA	37.58°N	118.23°W	3.801	Oct 1998 - Aug 2002	1.4×10^{15}	7.3×10^{15}
Ft. Sumner(FTS)	USA	34.48°N	104.22°W	1.260	Oct 1989 - Sep 2021	2.6×10^{16}	1.9×10^{16}
TMF, Wrightwood (TMF)	USA	34.38°N	117.68°W	2.257	Jul-Sep 1988; Nov 1996 Jan-Aug 1998; Oct 2009	2.7×10^{15}	8.3×10^{15}
JPL B183(JPL-B)	USA	34.20°N	118.17°W	0.345	Jun 1985 - Jan 2022	2.1×10^{16}	2.0×10^{16}
Xianghe	China	39.75°N	116.96°E	0.036	Jun 2018 - Jul 2022	1.8×10^{15}	3.0×10^{16}

systematic and random uncertainties of the C_3H_8 retrieved column are estimated to be 18.2% and 18.1%, respectively. In the C_3H_8 retrieval window, CH_4 and H_2O absorption lines are not perfectly fitted, indicating there is still room left to improving the line lists of these two species.

The mean and std of the C_3H_8 column derived from the FTIR measurements at Xianghe are $1.80 \pm 0.81 \times 10^{15}$ molec./cm². A month-to-month variation is observed with a high value in July and a low value in October. The difference between the median values in July (maximum) and October (minimum) is 1.2×10^{15} molec./cm². The FTIR C_3H_8 column retrievals are compared to two well-known models (CAM5 and WACCM). It is found that the mean C_3H_8 columns from the two models are 68% larger than the FTIR measurements at Xianghe, which is beyond the systematic uncertainty of our FTIR retrieval. Moreover, the seasonal variations of the C_3H_8 column derived from CAM5 and WACCM models also deviates from that derived from the FTIR measurements. Further investigations are needed to better understand the mismatch between the model simulations and FTIR measurements, and to improve the C_3H_8 model simulations at Xianghe.

As C_3H_8 are co-emitted with CH_4 , CO , C_2H_2 , and C_2H_6 during oil and gas production, we calculate the correlation between ΔC_3H_8 and these species at Xianghe. Good correlations are found between C_3H_8 and C_2H_6 , between C_3H_8 and C_2H_2 , as well as between C_3H_8 and CO . However, the correlation between C_3H_8 and CH_4 is relatively weak, which is probably due to CH_4 emission in North China being dominated by rice, cultivation, and waste, instead of oil and gas production and fossil fuels combustion. By comparing the C_3H_8 and C_2H_6 columns at Xianghe with 6 other sites around the world, provided by the ground-based MkIV spectrometers, we find that the C_2H_6 column at Xianghe is the largest. However, the C_3H_8 column at Xianghe is only larger than those observed at the mountain sites and polar sites, and it is much less than the C_3H_8 columns observed at mid-latitude sites in the USA.

In summary, we successfully retrieve C_3H_8 columns from the FTIR MIR spectra at Xianghe, which provides us with a new dataset to understand the variation of C_3H_8 in North China. The retrieval strategy of C_3H_8 in this study should work



at other Bruker 125HR FTIR sites as well, especially for those close to a city or oil and gas field, e.g., Paris, Toronto, and Boulder. Nevertheless, efforts are still needed within the NDACC-IWRG community to generate a global harmonized FTIR C_3H_8 column dataset.

Data availability. The ground-based MkIV C_3H_8 and C_2H_6 retrievals are publicly available via <https://mark4sun.jpl.nasa.gov/ground.html> (last access date: 27 September 2022). The FTIR C_3H_8 retrievals at Xianghe are available upon request. The CAMS model data are publicly available via <https://ads.atmosphere.copernicus.eu/> (last access date: 27 March 2024). The WACCM model data are publicly available via <https://www.acom.ucar.edu/waccm/download.shtml> (last access date: 27 March 2024).

Competing interests. The authors declare that they have no conflict of interest.

Acknowledgements. The author would like to thank the NDACC community for supporting the SFIT4 retrieval algorithm. We would acknowledge all Xianghe site staffs, Nicolas Kumps (BIRA-IASB) for the FTIR instrument maintenance. This study is supported by the National key research and development program (2023YFC3705202).

Author contributions. PW and MZ design the study and wrote the manuscript. MZ, BL, BD, MDM investigated the SFIT4 retrieval strategy. WN, CH and QC operate the FTIR measurements at Xianghe. GT provides the MKIV measurements. All authors have read and commented the manuscript.



References

- Blumenstock, T., Hase, F., Keens, A., Czurlok, D., Colebatch, O., Garcia, O., Griffith, D. W. T., Grutter, M., Hannigan, J. W., Heikkinen, P., Jeseck, P., Jones, N., Kivi, R., Lutsch, E., Makarova, M., Imhasin, H. K., Mellqvist, J., Morino, I., Nagahama, T., Notholt, J., Ortega, I., Palm, M., Raffalski, U., Rettinger, M., Robinson, J., Schneider, M., Servais, C., Smale, D., Stremme, W., Strong, K., Sussmann, R., Té, Y., and Velazco, V. A.: Characterization and potential for reducing optical resonances in Fourier transform infrared spectrometers of the Network for the Detection of Atmospheric Composition Change (NDACC), *Atmos. Meas. Tech.*, 14, 1239–1252, <https://doi.org/10.5194/amt-14-1239-2021>, 2021.
- 5 Boursoukoudis, E., Ernle, L., Crowley, J. N., Lelieveld, J., Paris, J.-D., Pozzer, A., Walter, D., and Williams, J.: Non-methane hydrocarbon (C_2 – C_8) sources and sinks around the Arabian Peninsula, *Atmos. Chem. Phys.*, 19, 7209–7232, [https://doi.org/10.5194/acp-19-7209-](https://doi.org/10.5194/acp-19-7209-2019)
- 10 2019, 2019.
- Callewaert, S., Zhou, M., Langerock, B., Wang, P., Wang, T., Mahieu, E., and De Mazière, M.: A WRF-Chem study on the variability of CO_2 , CH_4 and CO concentrations at Xianghe, China supported by ground-based observations and TROPOMI, *EGUsphere*, 2023, 1–37, <https://doi.org/10.5194/egusphere-2023-2103>, 2023.
- Crippa, M., Solazzo, E., Huang, G., Guizzardi, D., Koffi, E., Muntean, M., Schieberle, C., Friedrich, R., and Janssens-Maenhout, G.: High resolution temporal profiles in the Emissions Database for Global Atmospheric Research, *Sci. Data*, 7, 121, [https://doi.org/10.1038/s41597-](https://doi.org/10.1038/s41597-020-0462-2)
- 15 020-0462-2, 2020.
- De Mazière, M., Thompson, A. M., Kurylo, M. J., Wild, J. D., Bernhard, G., Blumenstock, T., Braathen, G. O., Hannigan, J. W., Lambert, J.-C., Leblanc, T., McGee, T. J., Nedoluha, G., Petropavlovskikh, I., Seckmeyer, G., Simon, P. C., Steinbrecht, W., and Strahan, S. E.: The Network for the Detection of Atmospheric Composition Change (NDACC): history, status and perspectives, *Atmos. Chem. Phys.*, 18, 4935–4964, [https://doi.org/10.5194/acp-18-4935-](https://doi.org/10.5194/acp-18-4935-2018)
- 20 2018, 2018.
- Donahue, N. M. and Prinn, R. G.: Nonmethane hydrocarbon chemistry in the remote marine boundary layer, *Journal of Geophysical Research: Atmospheres*, 95, 18 387–18 411, <https://doi.org/https://doi.org/10.1029/JD095iD11p18387>, 1990.
- Franco, B., Mahieu, E., Emmons, L. K., Tzompa-Sosa, Z. A., Fischer, E. V., Sudo, K., Bovy, B., Conway, S., Griffin, D., Hannigan, J. W., Strong, K., and Walker, K. A.: Evaluating ethane and methane emissions associated with the development of oil and natural gas extraction in North America, *Environ. Res. Lett.*, 11, 044 010, <https://doi.org/10.1088/1748-9326/11/4/044010>, 2016.
- 25 Gettelman, A., Mills, M. J., Kinnison, D. E., Garcia, R. R., Smith, A. K., Marsh, D. R., Tilmes, S., Vitt, F., Bardeen, C. G., McInerny, J., Liu, H.-L., Solomon, S. C., Polvani, L. M., Emmons, L. K., Lamarque, J.-F., Richter, J. H., Glanville, A. S., Bacmeister, J. T., Phillips, A. S., Neale, R. B., Simpson, I. R., DuVivier, A. K., Hodzic, A., and Randel, W. J.: The Whole Atmosphere Community Climate Model Version 6 (WACCM6), *J. Geophys. Res. Atmos.*, 124, 12 380–12 403, <https://doi.org/https://doi.org/10.1029/2019JD030943>, 2019.
- 30 Gordon, I., Rothman, L., Hargreaves, R., Hashemi, R., Karlovets, E., Skinner, F., Conway, E., Hill, C., Kochanov, R., Tan, Y., Weislo, P., Finenko, A., Nelson, K., Bernath, P., Birk, M., Boudon, V., Campargue, A., Chance, K., Coustenis, A., Drouin, B., Flaud, J., Gamache, R., Hodges, J., Jacquemart, D., Mlawer, E., Nikitin, A., Perevalov, V., Rotger, M., Tennyson, J., Toon, G., Tran, H., Tyuterev, V., Adkins, E., Baker, A., Barbe, A., Canè, E., Császár, A., Dudaryonok, A., Egorov, O., Fleisher, A., Fleurbaey, H., Foltynowicz, A., Furtenbacher, T., Harrison, J., Hartmann, J., Horneman, V., Huang, X., Karman, T., Karns, J., Kass, S., Kleiner, I., Kofman, V., Kwabia-Tchana, F., Lavrentieva, N., Lee, T., Long, D., Lukashovskaya, A., Lyulin, O., Makhnev, V., Matt, W., Massie, S., Melosso, M., Mikhailenko, S., Mondelain, D., Müller, H., Naumenko, O., Perrin, A., Polyansky, O., Raddaoui, E., Raston, P., Reed, Z., Rey, M., Richard, C., Tóbiás, R., Sadiq, I., Schwenke, D., Starikova, E., Sung, K., Tamassia, F., Tashkun, S., Vander Auwera, J., Vasilenko, I., Viganin, A., Villanueva,
- 35



- G., Vispoel, B., Wagner, G., Yachmenev, A., and Yurchenko, S.: The HITRAN2020 molecular spectroscopic database, *J Quant Spectrosc Radiat Transf.*, 277, 107949, <https://doi.org/https://doi.org/10.1016/j.jqsrt.2021.107949>, 2022.
- Harrison, J. J., Allen, N. D., and Bernath, P. F.: Infrared absorption cross sections for ethane (C₂H₆) in the 3 μ m region, *J. Quant. Spectrosc. Radiat. Transf.*, 111, 357–363, <https://doi.org/10.1016/J.JQSRT.2009.09.010>, 2010.
- 5 Hase, F., Hannigan, J., Coffey, M., Goldman, A., Höpfner, M., Jones, N., Rinsland, C., and Wood, S.: Intercomparison of retrieval codes used for the analysis of high-resolution, ground-based FTIR measurements, *J. Quant. Spectrosc. Radiat. Transf.*, 87, 25 – 52, <https://doi.org/10.1016/j.jqsrt.2003.12.008>, 2004.
- Inness, A., Ades, M., Agustí-Panareda, A., Barré, J., Benedictow, A., Blechschmidt, A.-M., Dominguez, J. J., Engelen, R., Eskes, H., Flemming, J., Huijnen, V., Jones, L., Kipling, Z., Massart, S., Parrington, M., Peuch, V.-H., Razinger, M., Remy, S., Schulz, M., and Suttie,
10 M.: The CAMS reanalysis of atmospheric composition, *Atmos. Chem. Phys.*, 19, 3515–3556, <https://doi.org/10.5194/acp-19-3515-2019>, 2019.
- IPCC: Climate change 2013: The physical science basis. Contribution of Working Group I to the Fifth Assessment Report of the Intergovernmental Panel on Climate Change, 2013.
- Jacob, D. J.: Introduction to Atmospheric Chemistry, Princeton University Press, <http://www.jstor.org/stable/j.ctt7t8hg>, 1999.
- 15 Ji, D., Zhou, M., Wang, P., Yang, Y., Wang, T., Sun, X., Hermans, C., Yao, B., and Wang, G.: Deriving Temporal and Vertical Distributions of Methane in Xianghe Using Ground-based Fourier Transform Infrared and Gas-analyzer Measurements, *Adv. Atmos. Sci.*, 37, 597–607, <https://doi.org/10.1007/s00376-020-9233-4>, 2020.
- Kort, E. A., Smith, M. L., Murray, L. T., Gvakharia, A., Brandt, A. R., Peischl, J., Ryerson, T. B., Sweeney, C., and Travis, K.: Fugitive emissions from the Bakken shale illustrate role of shale production in global ethane shift, *Geophys. Res. Lett.*, 43, 4617–4623,
20 <https://doi.org/https://doi.org/10.1002/2016GL068703>, 2016.
- Lelieveld, J., Evans, J. S., Fnais, M., Giannadaki, D., and Pozzer, A.: The contribution of outdoor air pollution sources to premature mortality on a global scale, *Nature*, 525, 367–371, <https://doi.org/10.1038/nature15371>, 2015.
- Li, M., Liu, H., Geng, G., Hong, C., Liu, F., Song, Y., Tong, D., Zheng, B., Cui, H., Man, H., Zhang, Q., and He, K.: Anthropogenic emission inventories in China: a review, *Natl. Sci. Rev.*, 4, 834–866, <https://doi.org/10.1093/nsr/nwx150>, 2017.
- 25 Li, M., Pozzer, A., Lelieveld, J., and Williams, J.: Northern hemispheric atmospheric ethane trends in the upper troposphere and lower stratosphere (2006–2016) with reference to methane and propane, *Earth Syst. Sci. Data*, 14, 4351–4364, <https://doi.org/10.5194/essd-14-4351-2022>, 2022.
- Loos, J., Birk, M., and Wagner, G.: Measurement of air-broadening line shape parameters and temperature dependence parameters of H₂O lines in the spectral ranges 1850–2280 cm⁻¹ and 2390–4000 cm⁻¹, *J. Quant. Spectrosc. Radiat. Transf.*, 203, 103–118,
30 <https://doi.org/10.1016/J.JQSRT.2017.03.033>, 2017.
- Marsh, D. R., Mills, M. J., Kinnison, D. E., Lamarque, J.-F., Calvo, N., and Polvani, L. M.: Climate Change from 1850 to 2005 Simulated in CESM1(WACCM), *J. Clim.*, 26, 7372–7391, <https://doi.org/10.1175/JCLI-D-12-00558.1>, 2013.
- Ortega, I., Buchholz, R. R., Hall, E. G., Hurst, D. F., Jordan, A. F., and Hannigan, J. W.: Tropospheric water vapor profiles obtained with FTIR: comparison with balloon-borne frost point hygrometers and influence on trace gas retrievals, *Atmos. Meas. Tech.*, 12, 873–890,
35 <https://doi.org/10.5194/amt-12-873-2019>, 2019.
- Pougatchev, N. S., Connor, B. J., and Rinsland, C. P.: Infrared measurements of the ozone vertical distribution above Kitt Peak, *J. Geophys. Res.*, 100, 16 689, <https://doi.org/10.1029/95JD01296>, 1995.



- Rigby, M., Montzka, S. A., Prinn, R. G., White, J. W. C., Young, D., O'Doherty, S., Lunt, M. F., Ganesan, A. L., Manning, A. J., Simmonds, P. G., Salameh, P. K., Harth, C. M., Mühle, J., Weiss, R. F., Fraser, P. J., Steele, L. P., Krummel, P. B., McCulloch, A., and Park, S.: Role of atmospheric oxidation in recent methane growth, *Proc. Natl. Acad. Sci.*, 114, 5373–5377, <https://doi.org/10.1073/pnas.1616426114>, 2017.
- 5 Rodgers, C. D.: *Inverse Methods for Atmospheric Sounding – Theory and Practice*, Series on Atmospheric Oceanic and Planetary Physics, vol. 2, World Scientific Publishing Co. Pte. Ltd, Singapore, <https://doi.org/10.1142/9789812813718>, 2000.
- Saha, S., Moorthi, S., Wu, X., Wang, J., Nadiga, S., Tripp, P., Behringer, D., Hou, Y.-T., ya Chuang, H., Iredell, M., Ek, M., Meng, J., Yang, R., Mendez, M. P., van den Dool, H., Zhang, Q., Wang, W., Chen, M., and Becker, E.: The NCEP Climate Forecast System Version 2, *J. Clim.*, 27, 2185 – 2208, <https://doi.org/10.1175/JCLI-D-12-00823.1>, 2014.
- 10 Saunio, M., Stavert, A. R., Poulter, B., Bousquet, P., Canadell, J. G., Jackson, R. B., Raymond, P. A., Dlugokencky, E. J., Houweling, S., Patra, P. K., Ciais, P., Arora, V. K., Bastviken, D., Bergamaschi, P., Blake, D. R., Brailsford, G., Bruhwiler, L., Carlson, K. M., Carrol, M., Castaldi, S., Chandra, N., Crevoisier, C., Crill, P. M., Covey, K., Curry, C. L., Etiope, G., Frankenberg, C., Gedney, N., Hegglin, M. I., Höglund-Isaksson, L., Hugelius, G., Ishizawa, M., Ito, A., Janssens-Maenhout, G., Jensen, K. M., Joos, F., Kleinen, T., Krummel, P. B., Langenfelds, R. L., Laruelle, G. G., Liu, L., Machida, T., Maksyutov, S., McDonald, K. C., McNorton, J., Miller, P. A., Melton, J. R.,
- 15 Morino, I., Müller, J., Murguía-Flores, F., Naik, V., Niwa, Y., Noce, S., O'Doherty, S., Parker, R. J., Peng, C., Peng, S., Peters, G. P., Prigent, C., Prinn, R., Ramonet, M., Regnier, P., Riley, W. J., Rosentreter, J. A., Segers, A., Simpson, I. J., Shi, H., Smith, S. J., Steele, L. P., Thornton, B. F., Tian, H., Tohjima, Y., Tubiello, F. N., Tsuruta, A., Viovy, N., Voulgarakis, A., Weber, T. S., van Weele, M., van der Werf, G. R., Weiss, R. F., Worthy, D., Wunch, D., Yin, Y., Yoshida, Y., Zhang, W., Zhang, Z., Zhao, Y., Zheng, B., Zhu, Q., Zhu, Q., and Zhuang, Q.: The Global Methane Budget 2000–2017, *Earth Syst. Sci. Data*, 12, 1561–1623, <https://doi.org/10.5194/essd-12-1561-2020>,
- 20 2020.
- Sepúlveda, E., Schneider, M., Hase, F., Barthlott, S., Dubravica, D., García, O. E., Gomez-Pelaez, A., González, Y., Guerra, J. C., Gisi, M., Kohlhepp, R., Dohe, S., Blumenstock, T., Strong, K., Weaver, D., Palm, M., Sadeghi, A., Deutscher, N. M., Warneke, T., Notholt, J., Jones, N., Griffith, D. W. T., Smale, D., Brailsford, G. W., Robinson, J., Meinhardt, F., Steinbacher, M., Aalto, T., and Worthy, D.: Tropospheric CH₄ signals as observed by NDACC FTIR at globally distributed sites and comparison to GAW surface in situ measurements, *Atmos. Meas. Tech.*, 7, 2337–2360, <https://doi.org/10.5194/amt-7-2337-2014>, 2014.
- 25 Sha, M. K., Langerock, B., Blavier, J.-F. L., Blumenstock, T., Borsdorff, T., Buschmann, M., Dehn, A., De Mazière, M., Deutscher, N. M., Feist, D. G., García, O. E., Griffith, D. W. T., Grutter, M., Hannigan, J. W., Hase, F., Heikkinen, P., Hermans, C., Iraci, L. T., Jeseck, P., Jones, N., Kivi, R., Kumps, N., Landgraf, J., Lorente, A., Mahieu, E., Makarova, M. V., Mellqvist, J., Metzger, J.-M., Morino, I., Nagahama, T., Notholt, J., Ohyama, H., Ortega, I., Palm, M., Petri, C., Pollard, D. F., Rettinger, M., Robinson, J., Roche, S., Roehl, C. M.,
- 30 Röhling, A. N., Rousogonous, C., Schneider, M., Shiomi, K., Smale, D., Stremme, W., Strong, K., Sussmann, R., Té, Y., Uchino, O., Velasco, V. A., Vrekoussis, M., Wang, P., Warneke, T., Wizenberg, T., Wunch, D., Yamanouchi, S., Yang, Y., and Zhou, M.: Validation of Methane and Carbon Monoxide from Sentinel-5 Precursor using TCCON and NDACC-IRWG stations, *Atmos. Meas. Tech.*, 14, 6249–6304, <https://doi.org/10.5194/amt-14-6249-2021>, 2021.
- Steck, T.: Methods for determining regularization for atmospheric retrieval problems, *Appl. Opt.*, 41, 1788–1797, <https://doi.org/10.1364/AO.41.001788>, 2002.
- Sze, N. D.: Anthropogenic CO Emissions: Implications for the Atmospheric CO-OH-CH₄ Cycle, *Science*, 195, 673–675, <https://doi.org/10.1126/science.195.4279.673>, 1977.



- Tan, J.-H., Guo, S.-J., Ma, Y.-L., Yang, F.-M., He, K.-B., Yu, Y.-C., Wang, J.-W., Shi, Z.-B., and Chen, G.-C.: Non-methane Hydrocarbons and Their Ozone Formation Potentials in Foshan, China, *Aerosol Air Qual. Res.*, 12, 387–398, <https://doi.org/10.4209/aaqr.2011.08.0127>, 2012.
- Thompson, C. R., Wofsy, S. C., Prather, M. J., Newman, P. A., Hanisco, T. F., Ryerson, T. B., Fahey, D. W., Apel, E. C., Brock, C. A., Brune, W. H., Froyd, K., Katich, J. M., Nicely, J. M., Peischl, J., Ray, E., Veres, P. R., Wang, S., Allen, H. M., Asher, E., Bian, H., Blake, D., Bourgeois, I., Budney, J., Bui, T. P., Butler, A., Campuzano-Jost, P., Chang, C., Chin, M., Commane, R., Correa, G., Crouse, J. D., Daube, B., Dibb, J. E., DiGangi, J. P., Diskin, G. S., Dollner, M., Elkins, J. W., Fiore, A. M., Flynn, C. M., Guo, H., Hall, S. R., Hannun, R. A., Hills, A., Hints, E. J., Hodzic, A., Hornbrook, R. S., Huey, L. G., Jimenez, J. L., Keeling, R. F., Kim, M. J., Kupc, A., Lacey, F., Lait, L. R., Lamarque, J.-F., Liu, J., McKain, K., Meinardi, S., Miller, D. O., Montzka, S. A., Moore, F. L., Morgan, E. J., Murphy, D. M., Murray, L. T., Nault, B. A., Neuman, J. A., Nguyen, L., Gonzalez, Y., Rollins, A., Rosenlof, K., Sargent, M., Schill, G., Schwarz, J. P., Clair, J. M. S., Steenrod, S. D., Stephens, B. B., Strahan, S. E., Strode, S. A., Sweeney, C., Thames, A. B., Ullmann, K., Wagner, N., Weber, R., Weinzierl, B., Wennberg, P. O., Williamson, C. J., Wolfe, G. M., and Zeng, L.: The NASA Atmospheric Tomography (ATom) Mission: Imaging the Chemistry of the Global Atmosphere, *Bull. Am. Meteorol. Soc.*, 103, E761 – E790, <https://doi.org/10.1175/BAMS-D-20-0315.1>, 2022.
- Tikhonov, A. N.: Solution of Incorrectly Formulated Problems and the Regularisation Method, *Soviet. Math. Dokl.*, 4, 1035–1038, 1963.
- Toon, G. C., Blavier, J.-F. L., Sung, K., and Yu, K.: Spectrometric measurements of atmospheric propane (C_3H_8), *Atmos. Chem. Phys.*, 21, 10727–10743, <https://doi.org/10.5194/acp-21-10727-2021>, 2021.
- Vigouroux, C., Langerock, B., Bauer Aquino, C. A., Blumenstock, T., Cheng, Z., De Mazière, M., De Smedt, I., Grutter, M., Hannigan, J. W., Jones, N., Kivi, R., Loyola, D., Lutsch, E., Mahieu, E., Makarova, M., Metzger, J.-M., Morino, I., Murata, I., Nagahama, T., Notholt, J., Ortega, I., Palm, M., Pinardi, G., Röhling, A., Smale, D., Stremme, W., Strong, K., Sussmann, R., Té, Y., van Roozendaal, M., Wang, P., and Winkler, H.: TROPOMI–Sentinel-5 Precursor formaldehyde validation using an extensive network of ground-based Fourier-transform infrared stations, *Atmos. Meas. Tech.*, 13, 3751–3767, <https://doi.org/10.5194/amt-13-3751-2020>, 2020.
- Wang, M., Shao, M., Chen, W., Lu, S., Liu, Y., Yuan, B., Zhang, Q., Zhang, Q., Chang, C.-C., Wang, B., Zeng, L., Hu, M., Yang, Y., and Li, Y.: Trends of non-methane hydrocarbons (NMHC) emissions in Beijing during 2002–2013, *Atmos. Chem. Phys.*, 15, 1489–1502, <https://doi.org/10.5194/acp-15-1489-2015>, 2015.
- Wofsy, S. C.: HIAPER Pole-to-Pole Observations (HIPPO): fine-grained, global-scale measurements of climatically important atmospheric gases and aerosols, *Philosophical Transactions of the Royal Society A: Mathematical, Physical and Engineering Sciences*, 369, 2073–2086, <https://doi.org/10.1098/rsta.2010.0313>, 2011.
- Xiao, Y., Logan, J. A., Jacob, D. J., Hudman, R. C., Yantosca, R., and Blake, D. R.: Global budget of ethane and regional constraints on U.S. sources, *J Geophys Res Atmos.*, 113, <https://doi.org/https://doi.org/10.1029/2007JD009415>, 2008.
- Yang, Y., Zhou, M., Langerock, B., Sha, M. K., Hermans, C., Wang, T., Ji, D., Vigouroux, C., Kumps, N., Wang, G., De Mazière, M., and Wang, P.: New ground-based Fourier-transform near-infrared solar absorption measurements of XCO_2 , XCH_4 and XCO at Xianghe, China, *Earth Syst. Sci. Data*, 12, 1679–1696, <https://doi.org/10.5194/essd-12-1679-2020>, 2020.
- Zhou, M., Vigouroux, C., Langerock, B., Wang, P., Dutton, G., Hermans, C., Kumps, N., Metzger, J.-M., Toon, G., and De Mazière, M.: CFC-11, CFC-12 and HCFC-22 ground-based remote sensing FTIR measurements at Réunion Island and comparisons with MIPAS/ENVISAT data, *Atmos. Meas. Tech.*, 9, 5621–5636, <https://doi.org/10.5194/amt-9-5621-2016>, 2016.
- Zhou, M., Langerock, B., Vigouroux, C., Sha, M. K., Ramonet, M., Delmotte, M., Mahieu, E., Bader, W., Hermans, C., Kumps, N., Metzger, J.-M., Dufлот, V., Wang, Z., Palm, M., and De Mazière, M.: Atmospheric CO and CH₄ time series and seasonal variations on



- Reunion Island from ground-based in-situ and FTIR (NDACC and TCCON) measurements, *Atmos. Chem. Phys.*, 18, 13 881–13 901, <https://doi.org/10.5194/acp-18-13881-2018>, 2018.
- Zhou, M., Wang, P., Langerock, B., Vigouroux, C., Hermans, C., Kumps, N., Wang, T., Yang, Y., Ji, D., Ran, L., Zhang, J., Xuan, Y., Chen, H., Posny, F., Duflo, V., Metzger, J.-M., and De Mazière, M.: Ground-based Fourier transform infrared (FTIR) O₃ retrievals from the 3040 cm⁻¹ spectral range at Xianghe, China, *Atmos. Meas. Tech.*, 13, 5379–5394, <https://doi.org/10.5194/amt-13-5379-2020>, 2020.
- Zhou, M., Langerock, B., Vigouroux, C., Dils, B., Hermans, C., Kumps, N., Nan, W., Metzger, J.-M., Mahieu, E., Wang, T., Wang, P., and De Mazière, M.: Tropospheric and stratospheric NO retrieved from ground-based Fourier-transform infrared (FTIR) measurements, *Atmos. Meas. Tech.*, 14, 6233–6247, <https://doi.org/10.5194/amt-14-6233-2021>, 2021.
- Zhou, M., Langerock, B., Wang, P., Vigouroux, C., Ni, Q., Hermans, C., Dils, B., Kumps, N., Nan, W., and De Mazière, M.: Understanding the variations and sources of CO, C₂H₂, C₂H₆, H₂CO, and HCN columns based on 3 years of new ground-based Fourier transform infrared measurements at Xianghe, China, *Atmos. Meas. Tech.*, 16, 273–293, <https://doi.org/10.5194/amt-16-273-2023>, 2023.